2nd IAA Conference on Space Situational Awareness (ICSSA)

Washington, DC, USA

IAA-ICSSA-20-0X-XX

Orbit Design for Cislunar Space Domain Awareness

Erin E. Fowler(1), **Stella B. Hurtt**(2), **Derek A. Paley**(3)

(1) *Department of Aerospace Engineering, University of Maryland, 8197 Regents Drive, Room 1141, College Park, MD 20742, efowler3@umd.edu*

(2) *Department of Aerospace Engineering, University of Maryland, College Park, MD 20742, shurtt1@umd.edu*

(3) *Department of Aerospace Engineering and Institute for Systems Research, University of Maryland College Park, 3150 Glenn L. Martin Hall, College Park, MD 20742, dpaley@umd.edu*

Keywords: *space-based cislunar domain awareness, observability*

This paper presents a quantitative assessments of the orbits and sensor characteristics of satellites intended for cislunar space domain awareness. A dynamic simulation of the cislunar environment enables a numerical analysis of various pairings of sensing satellites and resident space objects. Preliminary contributions include analysis of orbit families, including Earth orbits, Moon orbits, and L1 and L2 orbits, for their viability in the mission of space-based cislunar situational awareness. We propose a set of metrics for observability, including sensor considerations like occultation and lighting conditions, which can be used to inform the specific orbit parameterization for cislunar space domain awareness orbit design.

1. Introduction

Space domain awareness (SDA) and space traffic management (STM) are challenging due to an increasingly congested environment populated by a growing number of maneuverable vehicles and vehicles planned for deep space, i.e., beyond geosynchronous Earth orbit (GEO). Orbit design for the space-based cislunar domain awareness mission is an important topic due to the large range and limited viewing geometries between Earth-orbiting satellites and satellites in cislunar orbits. Complex astrodynamics must be modeled for objects in cislunar space, since lunar gravity cannot be neglected or treated as a perturbation to a dynamic model for cislunar object tracking, as it can in dynamic models of Earth-orbiting vehicles.

The cislunar regime is of increasing interest to the space industry due to its value for applications such as astronomy, interplanetary mission staging, lunar exploration and communications, and Earth orbit insertion [1]. Spacecraft placed in Earth-Moon collinear Lagrange points L1 and L2 avoid the gravity wells of the Earth and Moon, surface environmental issues, and artificial and natural space debris. These spacecraft require low stationkeeping propellant (on the order of centimeters per second) and can travel between L1 and L2 or between Earth-Moon space and Sun-Earth space [2].

In July 2019, a near-rectilinear halo orbit (NRHO) was chosen as the orbit for the future Lunar Gateway, which will be developed by the U.S. National Aeronautics and Space Administration (NASA) and the European Space Agency (ESA) to serve as a solar-powered communications hub, science laboratory, short-term habitation module, and holding area for rovers and other robots [1]. Cislunar orbits can also be used as storage locations for spare Earth-orbiting satellites, allowing responsive insertion of these spares into operational Earth orbits with none of the indications and warnings normally associated with launch of a new vehicle into Earth orbit [3]. Despite the desirable characteristics of certain cislunar orbits, NASA's ARTEMIS P1 (THEMIS B) and ARTEMIS P2 (THEMIS C) were the first two satellites to achieve orbit around an Earth-Moon Lagrange point as recently as 2010 [4]. As the opportunities offered by the cislunar regime become realities, space domain awareness and space traffic management specific to this environment will become increasingly critical capabilities. Preliminary results from this study could be used to inform the requirements for future cislunar space domain awareness systems, i.e., by placing satellites into specific orbits that maximize performance for SDA and STM missions.

Various models describe motion in the Earth-Moon system, including patched-conics approaches that switch among two-body models with the Earth, the Sun, and the Moon as central bodies; three-body models including the Earth and the Moon as primary masses; n-body models that directly incorporate the gravitational effects from more bodies than the two primaries; and models that incorporate perturbations like solar radiation pressure. A three-body model, which is used here, may be derived from a set of simplifying assumptions. The restricted three-body problem assumes that a body of negligible mass moves under the influence of two massive bodies, whereas the circular restricted three-body problem additionally assumes that the two primary masses move in nearly circular orbits about their barycenter. For the Earth-Moon system, these assumptions are valid since a large spacecraft of 5900 kg would have less than 10^{-16} times the force on the primaries that the primaries would have on each other, and the Moon's orbit has an eccentricity of only 0.055 [5]. The Circular Restricted Three-Body Problem (CR3BP) is used here as the basis for a dynamic simulation in which the relative motion of two satellites of negligible mass is studied.

The contributions of this paper are (1) the formulation of a preliminary set of metrics to describe the capability of a satellite performing a space domain awareness mission from an Earth-Moon system orbit to observe an object in another Earth-Moon system orbit; (2) parametric studies across Earth and Moon two-body orbital parameters to determine how satellites in these orbits may perform against these metrics; and (3) numerical examples to illustrate recommendations about the placement of satellites performing cislunar space domain awareness missions.

The paper's outline is as follows. Section 2 reviews the Circular Restricted Three-Body Problem (CR3BP) model of the Earth-Moon system, including a discussion of its utility in a study of the cislunar environment and the equilibrium points that can be found in the CR3BP model. Additionally, we list challenges for cislunar space domain awareness (SDA) and various types of orbits that exist in the Earth-Moon system. Section 3 describes our methodology, including the formulation of metrics and the set of observer orbits used for the study. Section 4 describes numerical results for Earth-orbiting observers of L1 and L2 orbiters and Moon-orbiting observers of L1 and L2 orbiters. Section 5 summarizes the paper and ongoing and future work.

2. Background

2.1. The Circular Restricted Three-Body Problem

Motion within the Earth-Moon system may be approximated using the dynamics of the Circular Restricted Three-Body Problem (CR3BP), in which the motion of a spacecraft with negligible mass is modeled under the influence of the gravitation of two primaries approximated as point masses [6]. By convention, the motion of the spacecraft is described using a coordinate system that rotates with the rate of rotation of the Earth and Moon in circular orbits about their barycenter. The planar CR3BP has two degrees of freedom, whereas the spatial CR3BP has three. Only one constant of motion exists, known as the Jacobi integral.

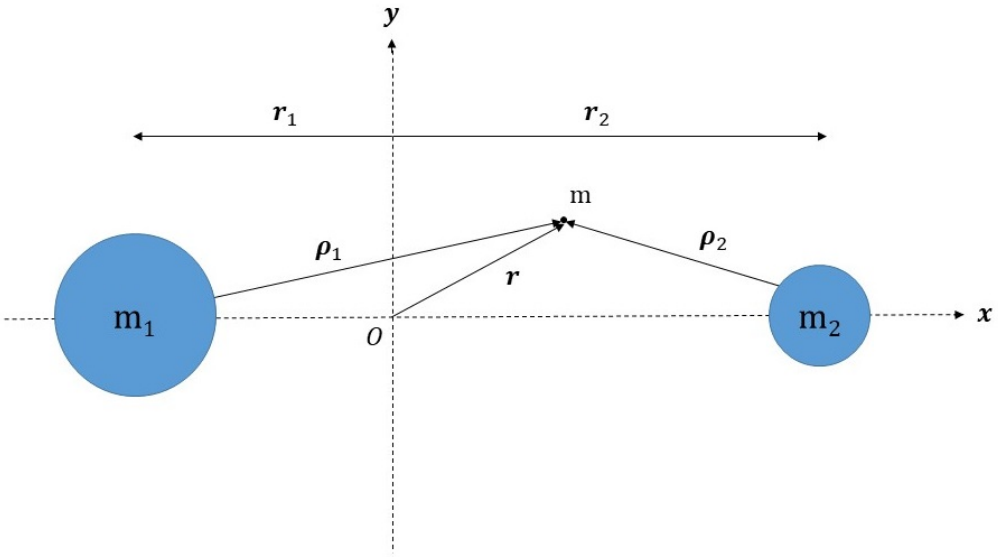

Figure 1: Circular Restricted Three-Body Problem. Mass m is a spacecraft of negligible mass compared to $m_1 \geq m_2$, which are two large primary masses.

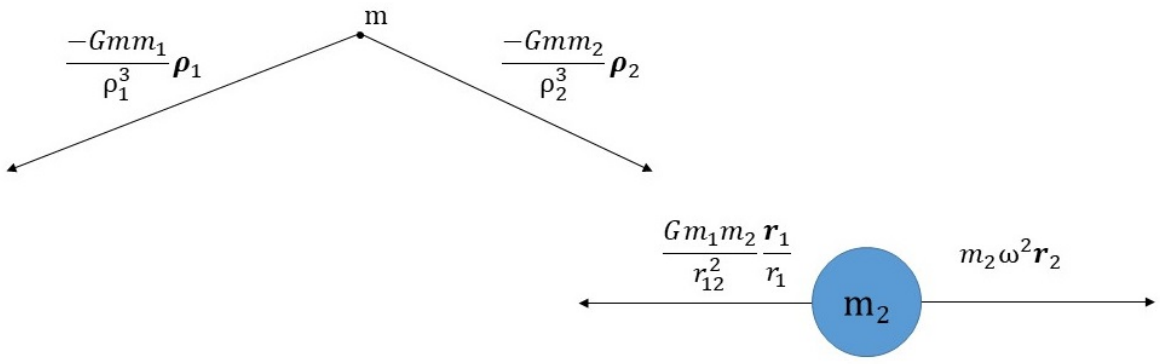

Figure 2: Free-body diagrams of spacecraft m (left) and smaller primary mass m_2 (right).

Since $\mathbf{r}_{CM} = \frac{m_1\mathbf{r}_1 + m_2\mathbf{r}_2}{m_1+m_2} = \mathbf{0}$, $r_1 = \frac{-m_2 r_2}{m_1} = \frac{-m_2}{m_1}(r_{12}+r_1)$, where $r_{12} = r_1 + r_2$, the constant distance between the two primaries m_1 and m_2, then $r_2 = \frac{m_1}{m_1+m_2} r_{12}$. Since the free-body diagram for m_2 shown in Fig. 2 gives $\frac{Gm_1m_2}{r_{12}^2} = m_2 r_2 \omega^2 = \frac{m_1 m_2}{m_1+m_2} r_{12}\omega^2$, the system shown in Fig. 1 rotates at a rate of [7]

$$\omega = \sqrt{\frac{G(m_1+m_2)}{r_{12}^3}}. \tag{1}$$

The free-body diagram for the spacecraft m in Fig. 2 provides the basis for the equations of motionin the CR3BP. Inertial acceleration $\mathbf{a}_i$ is $\mathbf{a}_i = \mathbf{a}_0 + \mathbf{a}_m + 2\boldsymbol{\omega} \times \mathbf{v} + \dot{\boldsymbol{\omega}} \times \mathbf{r} + \boldsymbol{\omega} \times (\boldsymbol{\omega} \times \mathbf{r})$, where $\mathbf{a}_0$ is the translational acceleration of the rotating frame, $\mathbf{a}_m$ is the acceleration of the spacecraft in the rotating frame, $2\boldsymbol{\omega} \times \mathbf{v}$ is Coriolis acceleration, $\dot{\boldsymbol{\omega}}$ is the time derivative of $\boldsymbol{\omega}$ with respect to the rotating frame, and $\boldsymbol{\omega} \times (\boldsymbol{\omega} \times \mathbf{r})$ is the centripetal acceleration. Because $\mathbf{a}_0$ and $\dot{\boldsymbol{\omega}} \times \mathbf{r}$ go to 0 and $\mathbf{a}_m = \ddot{\mathbf{r}}$, then

$$\ddot{\mathbf{r}} = \mathbf{a}_i - 2\boldsymbol{\omega} \times \mathbf{v} - \boldsymbol{\omega} \times (\boldsymbol{\omega} \times \mathbf{r}). \tag{2}$$

Since Newton's second law gives $\mathbf{a}_i = -G[\frac{m_1}{\rho_1^3}\rho_1 - \frac{m_2}{\rho_2^3}\rho_2]$, with $\rho_1 = \mathbf{r} - \mathbf{r}_1$ $= \begin{bmatrix} x - \frac{-m_2 r_{12}}{m_1+m_2} & y & z \end{bmatrix}^T$ and $\rho_2 = \mathbf{r} - \mathbf{r}_2 = \begin{bmatrix} x - \frac{m_1 r_{12}}{m_1+m_2} & y & z \end{bmatrix}^T$, and since the CR3BP rotates about the z axis in the frame shown in Fig. 1 (by convention in the $+z$ direction), giving $\boldsymbol{\omega} = \begin{bmatrix} 0 & 0 & \omega \end{bmatrix}^T$, Equation 2 becomes

$$\ddot{\mathbf{r}} = \frac{-Gm_1}{||\mathbf{r}-\mathbf{r}_1||}\begin{bmatrix} x + \frac{m_2}{m_1+m_2} r_{12} \\ y \\ z \end{bmatrix} - \frac{Gm_2}{||\mathbf{r}-\mathbf{r}_2||}\begin{bmatrix} x - \frac{m_1}{m_1+m_2} r_{12} \\ y \\ z \end{bmatrix} + 2\omega \begin{bmatrix} \dot{y} \\ -\dot{x} \\ 0 \end{bmatrix} + \omega^2 \begin{bmatrix} x \\ y \\ 0 \end{bmatrix}. \tag{3}$$

By convention, position, velocity, and mass are nondimensionalized in the CR3BP, so that the distance between the Earth and the Moon (r_{12}) becomes unity, as are the mean motion of the two primaries and the universal gravitational constant G [7]. The Earth's mass is denoted $1-\mu$, and the Moon's mass is μ. One distance unit is defined as $1DU \equiv r_{12}$, one mass unit as $1MU \equiv m_1 + m_2$ (so that mass ratio is $\mu = \frac{m_2}{m_1+m_2}$), and one time unit as $1TU \equiv \frac{T}{2\pi}$, where the orbital period T of the primaries about their barycenter is $T = \frac{2\pi}{\omega} = 2\pi\sqrt{\frac{r_{12}^3}{G(m_1+m_2)}}$ [8].

Using this nondimensionalization, the equations of motion for a spacecraft of negligible mass m from Equation 3 become [8]

$$\begin{bmatrix} \ddot{x} \\ \ddot{y} \\ \ddot{z} \end{bmatrix} = -\frac{(1-\mu)}{\rho_1^3}\begin{bmatrix} x+\mu \\ y \\ z \end{bmatrix} - \frac{\mu}{\rho_2^3}\begin{bmatrix} x-1+\mu \\ y \\ z \end{bmatrix} + \begin{bmatrix} 2\dot{y} \\ -2\dot{x} \\ 0 \end{bmatrix} + \begin{bmatrix} x \\ y \\ 0 \end{bmatrix}. \tag{4}$$

By convention, a state in the system with a positive ($+z$) angular momentum (such that the spacecraft is moving counter-clockwise in the Earth-Moon rotating frame) is considered prograde, whereas a clockwise motion is considered retrograde [9]. A solution in the CR3BP can be one of four types [10]: an equilibrium point, a periodic orbit (Lyapunov or halo), a quasi-periodic orbit (Lissajous), and chaotic. The halo orbits near the collinear Lagrange points L1 and L2 grow larger in size but shorter in period as they shift toward the Moon, and there exists a narrow band of halo orbits approximately halfway to the Moon from each of these two points that are of particular interest due to their stability characteristics [11].

Table 1: Non-dimensionalization constants in the Earth-Moon system

Unit	Variable	Value
Earth-Moon system orbital period	T	27.3215 days
Time unit	TU	4.348 days
Distance unit	DU	384400 km
Speed unit	SU	1.023 km/s
Mass ratio	μ	0.012277471

2.2. Equilibrium Points in the CR3BP

At equilibrium points in the CR3BP (known as Lagrange or libration points), gravitational and rotational accelerations balance [8]. At stable equilibrium points, perturbations cause oscillations about the equilibrium point, whereas at unstable equilibrium points, perturbations cause drift away from the equilibrium point. Equilibrium points occur where the gradient of the pseudopotential U vanishes, where

$$U = \frac{1}{2}\omega^2(x^2+y^2) + \frac{1-\mu}{\rho_1} + \frac{\mu}{\rho_2}, \tag{5}$$

so that

$$\begin{bmatrix} \ddot{x} \\ \ddot{y} \\ \ddot{z} \end{bmatrix} = \begin{bmatrix} 2\omega\dot{y} + \frac{\partial U}{\partial x} \\ -2\omega\dot{x} + \frac{\partial U}{\partial y} \\ \frac{\partial U}{\partial z} \end{bmatrix}. \tag{6}$$

When a spacecraft is at rest at an equilibrium point, $\dot{x} = \ddot{x} = \dot{y} = \ddot{y} = \dot{z} = \ddot{z} = 0$, which implies $\frac{\partial U}{\partial x} = \frac{\partial U}{\partial y} = \frac{\partial U}{\partial z} = 0$. Since $\frac{\partial U}{\partial z} = 0 = -z\mu((x-1+\mu)^2+y^2+z^2)^{-\frac{3}{2}}$, then $z = 0$ is the only solution, meaning that all Lagrange points lie in the xy plane of the rotating frame established in Fig. 1 [7].

Using U in terms of μ, ρ_1, and ρ_2, trivial solutions to $\frac{\partial U}{\partial x} = \frac{\partial U}{\partial \rho_1}\frac{\partial \rho_1}{\partial x} + \frac{\partial U}{\partial \rho_2}\frac{\partial \rho_2}{\partial x} = 0$ and $\frac{\partial U}{\partial y} = \frac{\partial U}{\partial \rho_1}\frac{\partial \rho_1}{\partial y} + \frac{\partial U}{\partial \rho_2}\frac{\partial \rho_2}{\partial y} = 0$ may be found. When $\frac{\partial U}{\partial \rho_1} = (1-\mu)(\rho_1 - \frac{1}{\rho_1^2})$ and $\frac{\partial U}{\partial \rho_2} = \mu(\rho_2 - \frac{1}{\rho_2^2})$ are set to 0, $\rho_1 = \rho_2 = 1$, meaning that the distances from the primaries to the spacecraft are the same and also equal to the distance between the primaries, forming an equilateral triangle. These points are known as L4 and L5 [7].

Stating x^2+y^2 in terms of μ, ρ_1, and ρ_2, Equation 5 becomes

$$U = (1-\mu)(\frac{\rho_1^2}{2} + \frac{1}{\rho_1}) + \mu(\frac{\rho_2^2}{2} + \frac{1}{\rho_2}) - \frac{\mu(1-\mu)}{2}. \tag{7}$$

To define the remaining equilibrium points (L1, L2, and L3), full solutions for $\frac{\partial U}{\partial x}$ and $\frac{\partial U}{\partial y}$ (and thus for $\frac{\partial \rho_1}{\partial x}$, $\frac{\partial \rho_1}{\partial y}$, $\frac{\partial \rho_2}{\partial x}$, $\frac{\partial \rho_2}{\partial y}$) are required. Given $\frac{\partial \rho_1}{\partial y} = \frac{y}{\rho_1}$ and $\frac{\partial \rho_2}{\partial y} = \frac{y}{\rho_2}$, the solution $\frac{\partial U}{\partial y} = (1-\mu)(\rho_1 - \frac{1}{\rho_1^2})(\frac{y}{\rho_1}) + \mu(\rho_2 - \frac{1}{\rho_2^2})(\frac{y}{\rho_2}) = 0$ reveals that $y = 0$ for the remaining equilibrium points L1, L2, and L3, described as the collinear Lagrange points. Given $\frac{\partial \rho_1}{\partial x} = \frac{x+\mu}{\rho_1}$ and $\frac{\partial \rho_2}{\partial x} = \frac{x-1+\mu}{\rho_2}$, the positions of L1, L2, and L3 along the x axis are found from the solution $\frac{\partial U}{\partial x} = (1-\mu)(\rho_1 - \frac{1}{\rho_1^2})(\frac{x+\mu}{\rho_1}) + \mu(\rho_2 - \frac{1}{\rho_2^2})(\frac{x-1+\mu}{\rho_2}) = 0$, i.e.,

$$\begin{aligned} x_{L1} &= (1-\mu) - \rho_2 \\ x_{L2} &= \rho_2 + (1-\mu) \\ x_{L3} &= -\rho_1 - \mu. \end{aligned} \tag{8}$$

The solutions to Equations 8 are found numerically as functions of mass ratio μ.

See Fig. 3 for a depiction of the geometry of the Lagrange points. In the Earth-Moon system, L4 and L5 are stable equilibrium points, whereas L1, L2, and L3 are unstable.

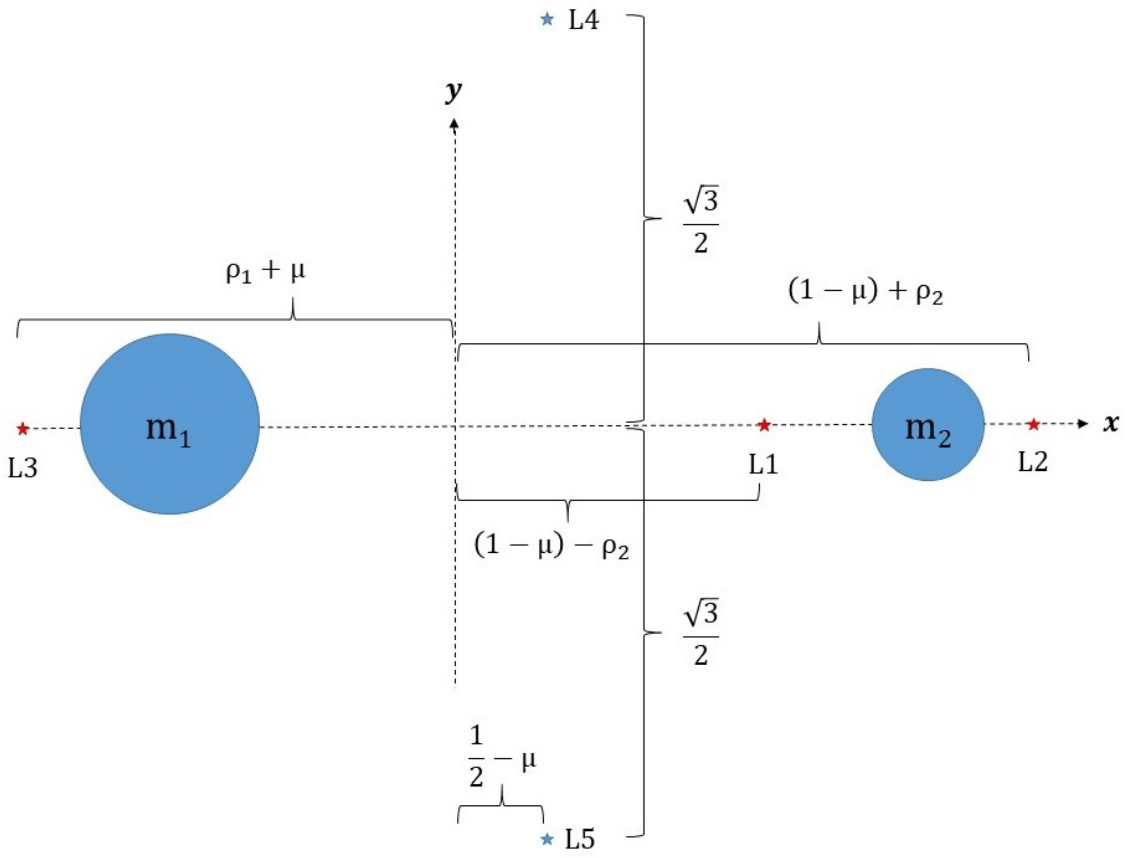

Figure 3: Locations of Lagrange points for the CR3BP. L4 and L5 are stable equilibrium points, whereas L1, L2, and L3 are unstable.

2.3. Challenges for Cislunar Space Domain Awareness

Objects in cislunar orbits are approximately ten times farther from the Earth's surface than objects being tracked in geostationary/geosynchronous earth orbits (GEO/GSO) [12]. Given current technology, optical systems based on the Earth's surface are capable of detecting only very large objects (hundreds of meters in size) at those distances. Deep space missions for science and exploration have used cooperative methods for orbit determination (e.g., two-way Doppler tracking) at these and larger ranges, but for space domain awareness and space traffic management purposes, cooperative methods cannot be assumed [13].

Additionally, objects in cislunar space appear to move very slowly from the perspective of an observer based on the Earth's surface or even orbiting the Earth, such that there may be insufficient geometric diversity in the observations for the observer to detect motion and create an orbit estimate. Objects in the cislunar environment can also spend significant time in front of or behind the Moon, or within a Sun- or Moon-exclusion angle with respect to an observer's sensor, which could cause an observer

to lose custody of the object. These considerations form the basis for the metrics proposed in Section 3.

2.4. Cislunar Orbits

Lyapunov orbits and halo orbits are periodic motions about the collinear Earth-Moon Lagrange points (L1, L2, L3). Lyapunov orbits lie entirely in the plane of the two primary bodies (the xy plane shown in Fig. 1), whereas halo orbits include an out-of-plane component. Orbits about Earth-Moon L2, for example, are called halo orbits when the size of the orbit is comparable to the distance of L2 from the Moon, resulting in periodic three-dimensional motion. L2 halo orbits require relatively low ΔV to reach from Earth and have continuous Earth visibility since they are always perpendicular to the Earth-Moon plane with amplitudes larger than the radius of the Moon [9]. The CR3BP orbits considered in this paper include Lyapunov orbits about L1 and L2. In ongoing and future work, we plan to examine a distant retrograde orbit (DRO), a halo orbit, and a near-rectilinear halo orbit (NRHO), which is a specific type of halo orbit of interest due to favorable stability properties for long-term missions and favorable resonance properties that avoid eclipses [14].

3. Methodology

3.1. Observability Metrics

In order to use a CR3BP dynamic simulation to analyze various orbit pairings, we define several observability metrics. Since an estimate of the orbit of an object is based on observations, the object must have some apparent motion with respect to the observer [15]. The first metric is the inverse of the relative angular rate, defined as hours per degree of motion of the observed object from the perspective of the observer. A lower value for this metric represents a more observable orbit.

Other viewing geometry concerns, like occultation by the Earth or Moon and Sun exclusion angles for optical sensors, reduce the amount of time that an object of interest is viewable by the observer. Therefore, the second metric is the percentage of the orbital period of the object when it is unavailable to the observer for any of these reasons. A lower value for this metric represents a more observable orbit. Earth and Moon positions are given in the CR3BP, and we added the Sun's position by assuming a mission start date of January 1, 2010 and downloading Sun ephemeris data with respect to the Earth-Moon barycenter from the JPL Horizons database (https://ssd.jpl.nasa.gov/horizons.cgi).

Finally, we consider the large range from the observer to the object being observed. Given that objects in orbit around or near the Moon are approximately ten times farther from Earth than the farthest objects being tracked for other space domain awareness efforts (i.e., objects in GEO), range is a critical third metric that can be reduced by prudent placement of space-based assets.

3.2. Observer Orbits

In the CR3BP dynamic simulation, we placed objects in Lyapunov orbits about L1 and L2, i.e., entirely in the plane of the Earth-Moon system. We used these objects as the targets of interest to assess various Earth-orbiting and Moon-orbiting observers using the SDA metrics above. We postulate that, for the purpose of observing these objects, Moon observing orbits may show greater promise than Earth observing orbits.

The six Keplerian orbital elements (except eccentricity) are shown in Fig. 4. Two of these parameters define the size and shape of a two-body orbit: the eccentricity e describes how elongated an elliptical orbit is compared to a circle ($e = 0$ for a circular orbit), and the semimajor axis a is the arithmetic mean of the periapsis and apoapsis distances (the orbit's radius for a circular orbit). Two parameters describe the orientation of the orbital plane in which the ellipse is embedded: the inclination i describes the vertical tilt of the ellipse with respect to the reference plane, measured at the ascending node (where the orbit passes from below through the reference plane), and the longitude of ascending node Ω horizontally orients the ascending node of the ellipse with respect to the reference frame's vernal point (symbolized by Υ). Finally, two parameters describe the orientation of the ellipse within its orbital plane and the (time-varying) position of an object along its orbit: the argument of periapsis ω defines the orientation of the ellipse in the orbital plane as an angle measured from the ascending node to periapsis, and the true anomaly ν defines the position of the orbiting body along the ellipse at a specific time (epoch). All Keplerian orbital elements are constant for a given orbit except the true anomaly ν [12].

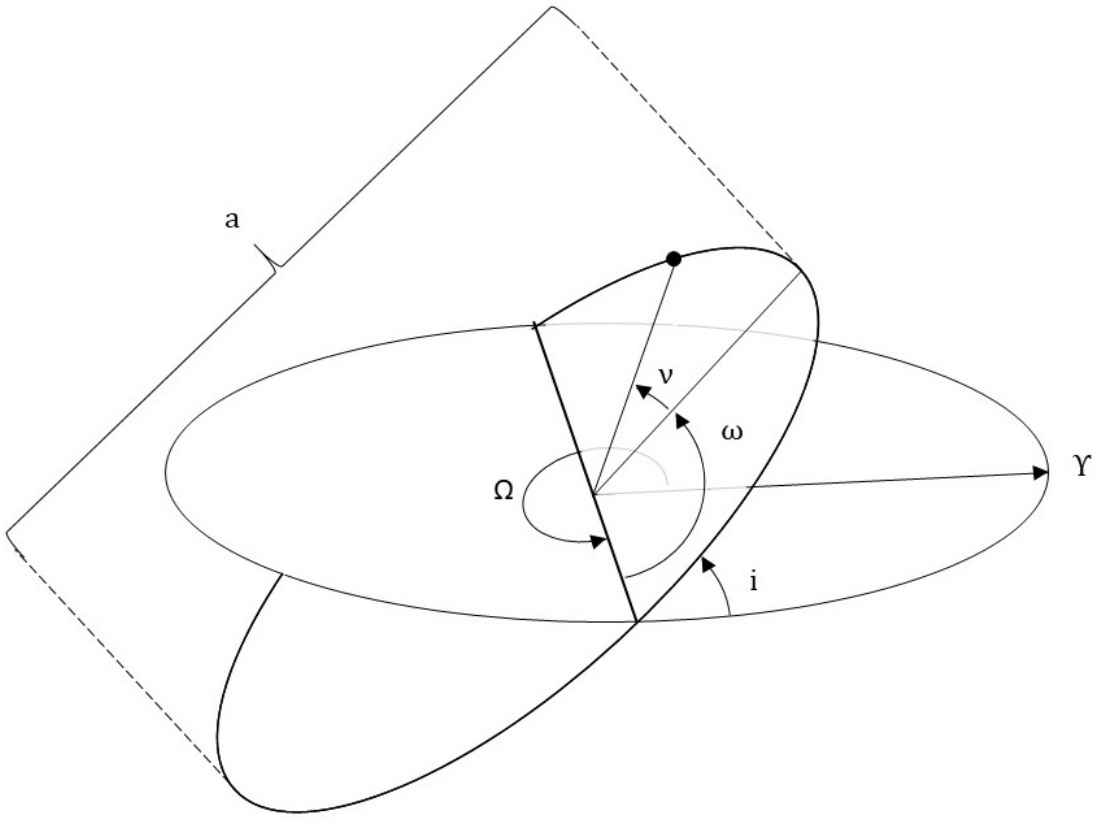

Figure 4: Keplerian orbital elements (except eccentricity e).

For our parametric analysis of Earth and Moon observing orbits, we varied eccentricity e, semimajor axis a, and inclination i about nominal values to discern how these variations would affect our metrics. Fig. 5 depicts the geometry of a representative system with Lyapunov orbits about L1 and L2 and an observer orbit about Earth with $a = 24832$ km, $e = 0.225$, and $i = 20^\circ$, propagated for 120 days.

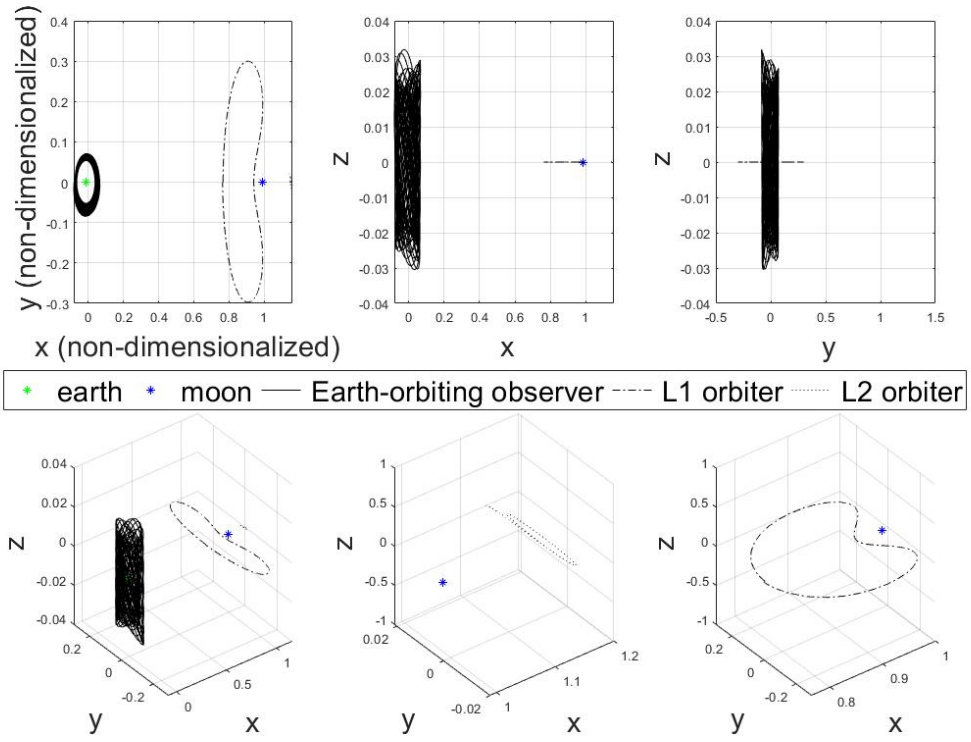

Figure 5: Geometry of the Earth-Moon system with Lyapunov orbits about L1 and L2 and a representative observer orbit about Earth with semimajor axis 24832 km, eccentricity 0.225, and inclination 20°.

4. Results

First, we analyze the effectiveness of an Earth orbiter for observing objects in these L1 and L2 Lyapunov orbits, shown in Fig. 6. General trends can be seen for all three metrics. Interestingly, for some of the parameters considered, the first and third metrics trend in opposite directions with variations in the orbital parameters from nominal values. This trade off makes intuitive sense when the geometry of a distant observation problem is considered: the farther from the viewer an object is, the more slowly it appears to move from the perspective of the viewer.

Additionally, we analyze the effectiveness of a Moon orbiter for the purpose of observing objects in the same L1 and L2 Lyapunov orbits, shown in Fig. 7. A Moon orbiter shows superior performance over an Earth orbiter for the mission of observing an L1 orbiter since the time it takes the L1 orbiter to pass through 1° from the perspective of the observer is more than an order of magnitude less than the time it takes the same orbiter to pass through 1° from the perspective of an Earth orbiter. Additionally, the L1 orbiter is unavailable for observation by a Moon-orbiting observer near 20% of the time as compared to the approximately 65% of the time for an Earth orbiter, and the average distance from the Moon orbiting observer to the L1 orbiter is almost an order of magnitude smaller than for the Earth-orbiting observer.

A Moon orbiter observing an L2 orbiter shows undesirably large values near 80% for the percentage of time when the L2 orbiter is unavailable for observation by the Moon

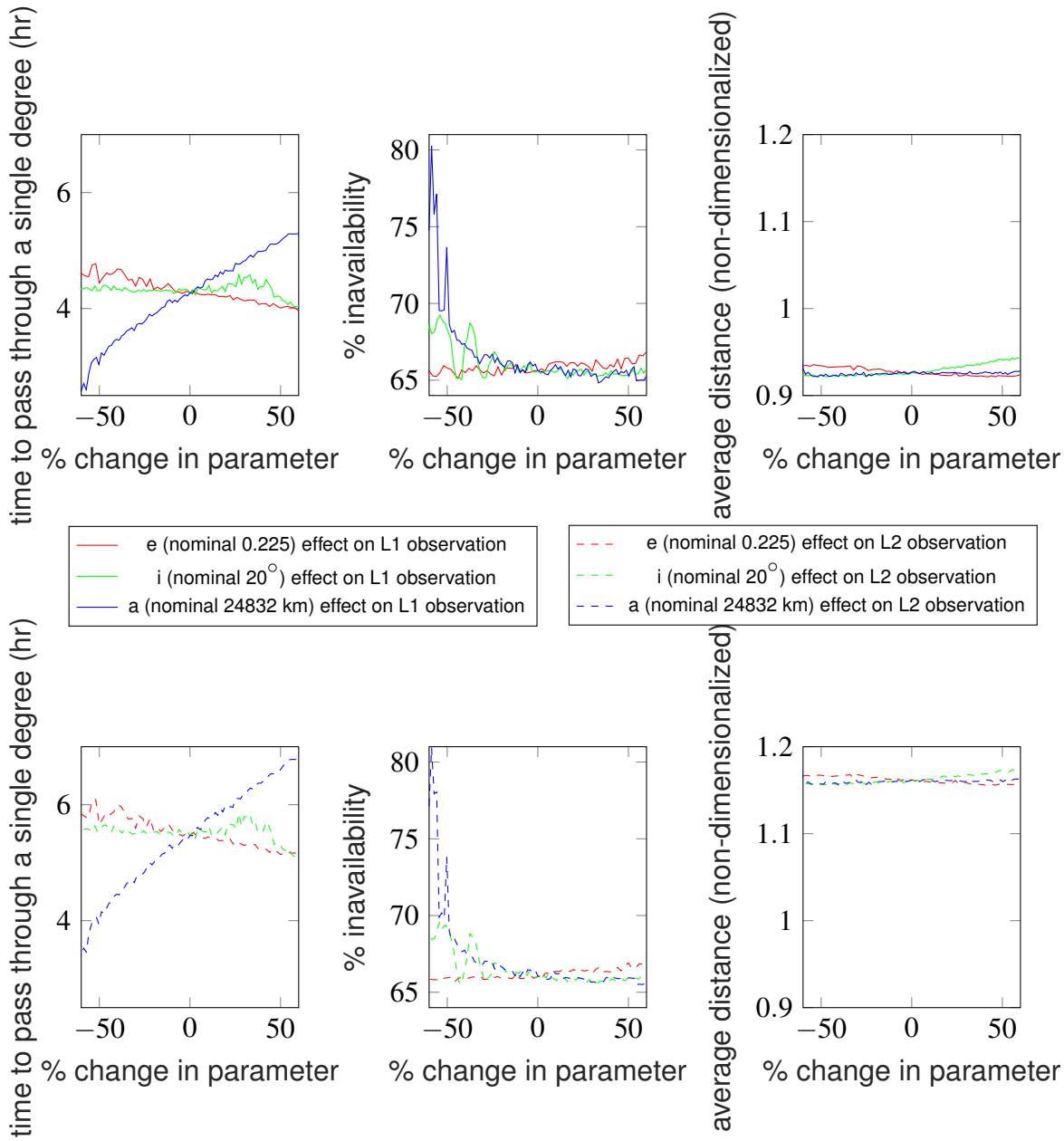

Figure 6: Results for an Earth orbiter observing L1 and L2 orbiters. The time it takes the observed object to pass through a single degree and the average distance to the object show trends with variations in the orbital elements, whereas % inavailability shows no clear trend with the same variations.

orbiter because of the relative position of the Sun during the simulation time. The Sun is almost directly behind L2 from the perspective of the Moon for most of the time. Due to geometry, this means the Sun is also almost directly behind L1, the Moon, and L2 from the perspective of the Earth, explaining why the values for percentage inavailability are also large for an Earth orbiter observing L1- and L2-orbiters. A Moon orbiter observing an L2 orbiter also shows about a two times improvement over an Earth orbiter in first metric and almost an order of magnitude improvement in average distance.

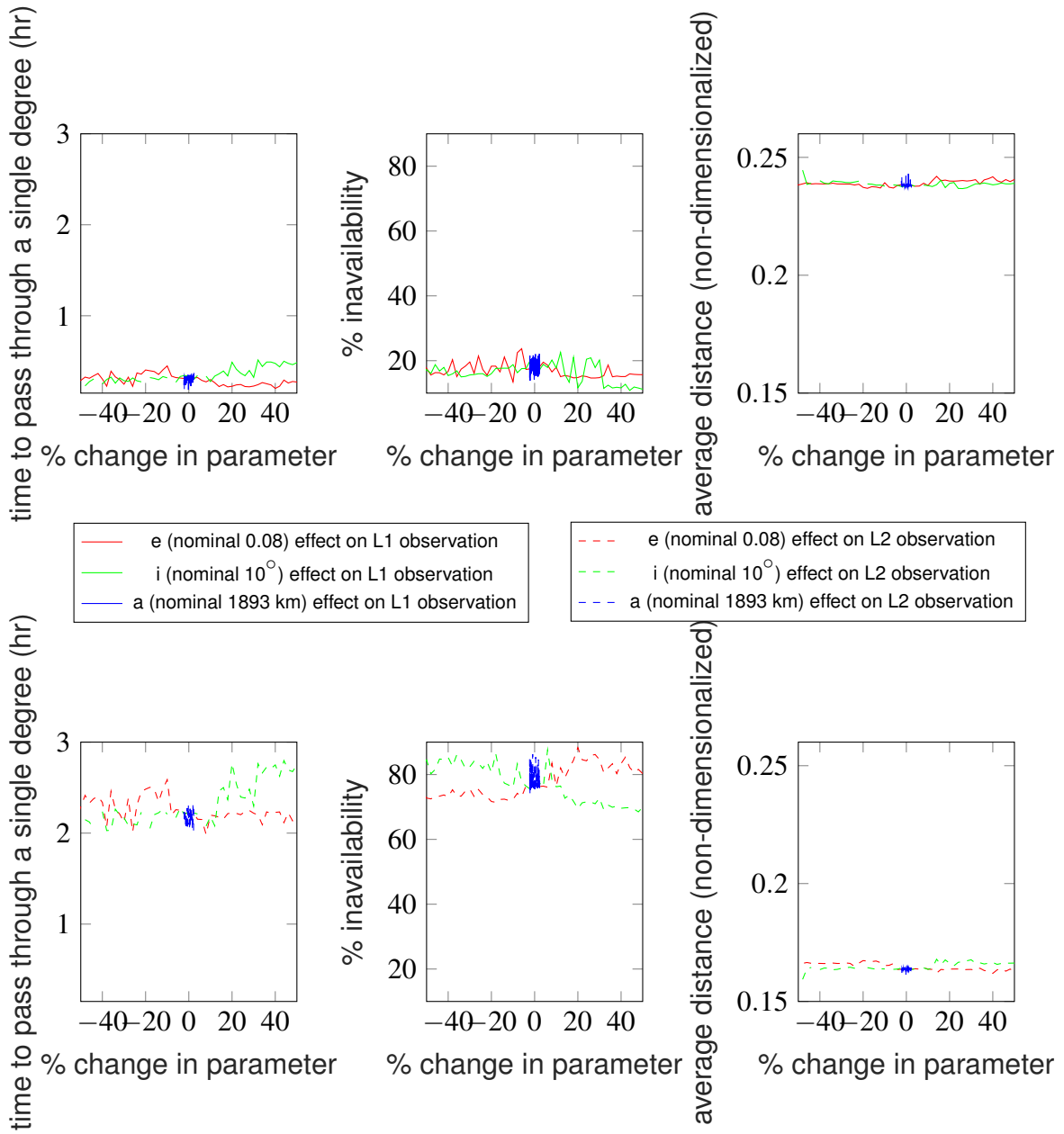

Figure 7: Results for a Moon orbiter observing L1 and L2 orbiters. The metrics show trends with variations in eccentricity e and inclination i; semi-major axis a is not varied enough within the dynamic simulation to produce a trend.

5. Conclusion

This paper presents a set of three performance metrics to describe the capability of a satellite performing a space domain awareness mission from an Earth-Moon system orbit to observe an object in a different Earth-Moon system orbit. Parametric studies across Earth and Moon two-body orbital parameters determine how satellites in these orbits perform. Numerical examples illustrate recommendations about the placement of satellites performing cislunar space domain awareness missions. According to the metrics chosen, Moon orbits are a dramatically better choice for the mission of observing L1- and L2-orbiting objects than Earth orbits, and using an Earth

orbiter for this mission would require a trade between the observer's performance on two of three metrics. Ongoing and future work includes consideration of additional orbits both for observers and objects to be observed. For instance, an orbiter about one of the triangular points (L4 or L5) is likely to perform well when observing orbiters of L1 and L2.

Acknowledgments

E. Fowler is supported by the U.S. Naval Research Laboratory Edison Memorial Graduate Training Program.

References

[1] S. Lizy-Destrez, L. Beauregard, E. Blazquez, S. Manglativi, V. Quet, Rendezvous strategies in the vicinity of earth-moon lagrangian points, Frontiers in Astronomy and Space Sciences 5 (2019) 1–19.

[2] M. R. Bobskill, M. L. Lupisella, The role of cis-lunar space in future global space exploration, in: Proceedings of the Global Space Exploration Conference, Washington, District of Columbia, pp. 1–15. May 22–24, 2012. Paper number GLEX-2012.05.5.4x12270.

[3] J. Chase, N. Chow, E. Gralla, N. J. Kasdin, Leo constellation design using the lunar l1 point, in: Proceedings of the 14th AAS/AIAA Space Flight Mechanics Meeting, Maui, HI, pp. 1–19. February 8–12, 2004. Paper number AAS 04-248.

[4] T. A. Pavlak, K. C. Howell, Evolution of the out-of-plane amplitude for quasi-periodic trajectories in the earth-moon system, Acta Astronautica 81 (2012) 456–465.

[5] B. L. Jones, A Guidance and Navigation System For Two Spacecraft Rendezvous in Translunar Halo Orbit, Ph.D. thesis, University of Texas at Austin, Austin, TX 78712, 1993.

[6] W. S. Koon, M. W. Lo, J. E. Marsden, S. D. Ross, Dynamical Systems, the Three-Body Problem and Space Mission Design, Springer, 2007.

[7] J. M. A. Danby, Fundamentals of Celestial Mechanics, Willmann-Bell, 2nd edition, 1992.

[8] A. E. Roy, Orbital Motion, Taylor & Francis Group, 4th edition, 2005.

[9] J. S. Parker, R. L. Anderson, Low-Energy Lunar Trajectory Design, Wiley, 1st edition, 2014.

[10] G. Gomez, J. Llibre, R. Martinez, C. Simo, Dynamics and Mission Design Near Libration Points, Fundamentals: The Case of Collinear Libration Points, volume 2 of *World Scientific Monograph Series in Mathematics*, World Scientific Publishing, 2001.

[11] J. V. Breakwell, J. V. Brown, The halo family of 3-dimensional periodic orbits in the earth-moon restricted 3-body problem, Celestial Mechanics 20 (1979) 389–404.

[12] R. R. Bate, D. D. Mueller, J. E. White, Fundamentals of Astrodynamics, Dover, 1971.

[13] M. Beckman, Orbit determination issues for libration point orbits, in: Proceedings of the International Conference of Libration Point Orbits and Applications, Girona, Spain, pp. 1–9. June 10–14, 2002. Paper number 20020081023.

[14] E. M. Zimovan, K. C. Howell, D. C. Davis, Near rectilinear halo orbits and their application in cis-lunar space, in: Proceedings of the 3rd IAA Conference on Dynamics and Controls of Space Systems, Moscow, Russia, pp. 1–20. May 30–June 1, 2017. Paper number IAA-AAS-DyCoSS3-125.

[15] D. A. Vallado, Fundamentals of Astrodynamics and Applications, Microcosm Press and Kluwer Academic Publishers, 2nd edition, 2001.